Segmentation-driven optimization for iterative reconstruction in optical projection tomography: an exploration

Tang, X.; Spaink, H.A.J.; Wijk, R.C. van; Verbeek, F.J.

Segmentation-Driven Optimization For Iterative Reconstruction in Optical Projection Tomography: An Exploration

Xiaoqin Tang, Hermes A. J. Spaink, Rob C. van Wijk, and Fons J. Verbeek

***Abstract*—Three-dimensional reconstruction of tomograms from optical projection microscopy is confronted with several drawbacks. In this paper we employ iterative reconstruction algorithms to avoid streak artefacts in the reconstruction and explore possible ways to optimize two parameters of the algorithms, i.e., iteration number and initialization, in order to improve the reconstruction performance. As benchmarks for direct reconstruction evaluation in optical projection tomography are absent, we consider the assessment through the performance of the segmentation on the 3D reconstruction. In our explorative experiments we use the zebrafish model system which is a typical specimen for use in optical projection tomography system; and as such frequently used. In this manner data can be easily obtained from which a benchmark set can be built. For the segmentation approach we apply a two-dimensional U-net convolutional neural network because it is recognized to have a good performance in biomedical image segmentation. In order to prevent the training from getting stuck in local minima, a novel learning rate schema is proposed. This optimization achieves a lower training loss during the training process, as compared to an optimal constant learning rate. Our experiments demonstrate that the approach to the benchmarking of iterative reconstruction via results of segmentation is very useful. It contributes an important tool to the development of computational tools for optical projection tomography.**

***Index Terms*—Image reconstruction, Image segmentation, Deep learning, Convolutional neural network, OPT.**

I. Introduction

OPTICAL projection tomography (OPT) is an imaging technique from which three-dimensional (3D) images can be obtained. It is typically for objects in the size range of millimeters. Images are acquired over a full revolution of an object: i.e., the tomogram. The OPT microscope is configured such that this can be accomplished. Using computational techniques, a 3D volumetric image is obtained. OPT can play a crucial role in providing insight into protein distribution and/or gene expression within model organisms, such as zebrafish (*Danio rerio*), at a tissue and organ level, with the structures/objects of interest fluorescently labeled [1], [2]. Given the specific data a simple reconstruction technique may introduce artefacts that hamper the interpretation of the image. These artefacts are introduced as a part of the reconstruction process because of imperfections in the data prior to the imaging process. There are two possible approaches to reduce or eliminate these artefacts. The first is from the perspective of the imaging process itself, i.e., trying to avoid the imaging imperfections that results in artefacts, either from the sample side or from the instrument side. This approach can, however, sometimes be quite expensive or difficult to achieve. The second category is to improve the reconstruction from an imperfect tomogram through computational approaches. This can be accomplished by either applying a powerful reconstruction algorithm or by employing a pre- and/or post-processing of a specific algorithm.

In 2005, Walls *et al.* [3] presented the possible artefacts of Filtered Back Projection (FBP) reconstruction from an OPT imaging system. The main contribution of this work lies in the study of the provenance of reconstruction artefacts from the imaging source such as signal decay, imperfections of the charge-coupled device (CCD), etc. The reasons for these imperfections in imaging to result in reconstruction artefacts within the FBP [4] framework were investigated. It could, however, not yet explain if more advanced reconstruction algorithms, such as iterative reconstruction, reduce or even eliminate these artefacts.

A major artefact in OPT imaging with FBP reconstruction are the so-called streak artefacts. Compared to high-resolution microscopes, e.g., confocal microscopy [5], [6], OPT imaging is characterized by its wide depth of field (DoF). This means that a point source that is properly focused at one angle of rotation may be blurred or even invisible in the opposite angle [7]. This introduces a severe asymmetry in the tomograms and results in the before mentioned streak artefacts during FBP reconstruction. Fig. 1 shows an example of streak artefacts in the 3D reconstruction of a zebrafish sample. With different reconstruction algorithms implemented on the same imperfect data, completely different results are obtained.

Iterative reconstruction [8]–[11] refers to iterative algorithmic approaches used to reconstruct 2D or 3D images from tomographic imaging techniques. In general, it starts with an assumed image, then projections are computed from that

Manuscript received March 20, 2020; revised July 10, 2020 and September 19, 2020; accepted October 29, 2020. Date of publication November 17, 2020; date of current version December 4, 2020. This work was supported by China Scholarship Council (CSC). The associate editor coordinating the review of this manuscript and approving it for publication was Dr. Ilaria Catapano. *(Corresponding author: Xiaoqin Tang.)*

Xiaoqin Tang, Hermes A. J. Spaink, and Fons J. Verbeek are with the Leiden Institute t of Advanced Computer Science, Leiden University, Leiden 2333, The Netherlands (e-mail: x.tang@liacs.leidenuniv.nl; f.j.verbeek@liacs.leidenuniv.nl; hermes.spaink@gmail.com).

Rob C. van Wijk is with the Department of Pharmaceutial Biosciences, Uppsala University, 752 37 Uppsala, Sweden (e-mail: rob.vanwijk@farmbio.uu.se).

Digital Object Identifier 10.1109/TCI.2020.3038489

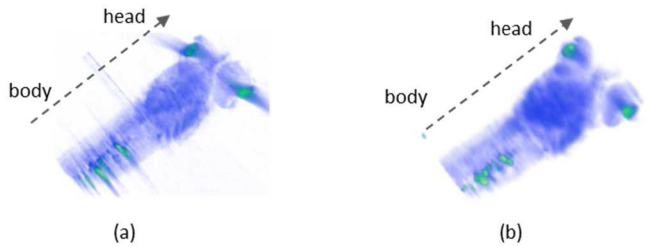

Fig. 1. (a) 3D volume rendering with streak artefacts after application of FBP reconstruction on a zebrafish sample. (b) 3D volume rendering with no streak artefacts after application of an iterative reconstruction on the same sample.

image via a projection function and an update of the image is established according to the difference between the calculated and the actual projections. With respect to the updating schema for the image, four kinds of approaches are distinguished, i.e., algebraic reconstruction techniques (ART) [12], iterative sparse asymptotic minimum variance (SAMV) [13], statistical reconstruction [14] and learned iterative reconstruction [15], [16]. These algorithms are considered superior when there is a lack of uniform projections or when the projections are sparse, which to some extent fits the character of OPT imaging causing the aforementioned streak artefacts. Compared to OPT, iterative reconstruction was mostly studied in the application area of computed tomography (CT) [8], [10], [11]. In 2015 Correia *et al.* [17] applied the iterative reconstruction to achieve relatively reasonable results on a sparse collection of projections. Iterative algorithms require a lot of computation time and this is one possible reason for hampering prevalence in OPT. Nevertheless, with the rapid development of smart computational strategies, e.g., parallel and graphics processing unit (GPU) computing, iterative reconstruction will become more widely applicable in OPT.

In the iterative reconstruction framework, reconstruction parameters are experimentally determined by experience and prior knowledge [8], [9], [11], [18]. This can be accomplished by visually comparing reconstructions resulting from different parameters. Because of the differences in data perception, the selection of parameters is subjective with respect to the background and knowledge of the experts. This might bring about a parameter set that is far from optimal. In order to achieve a desired outcome of reconstruction, quantitative tuning of the parameters is necessary.

The common approach for the evaluation of reconstruction performance in tomographic imaging is accomplished by producing and projecting a simulated object, i.e., a phantom object in CT, and assessing the performance of a reconstruction algorithm based on the projections [19]. Nevertheless, due to the DoF and the requirement of transparency in OPT imaging the projection function is much more complicated than that in CT imaging. In this case, simulating the projections of a phantom as benchmark has, to the best of our knowledge, never happened in OPT. As an alternative, we therefore use images from real-life samples as in an experimental evaluation setup.

Despite of its potential in image reconstruction, iterative reconstruction is, however, not exempt from an intrinsic difficulty

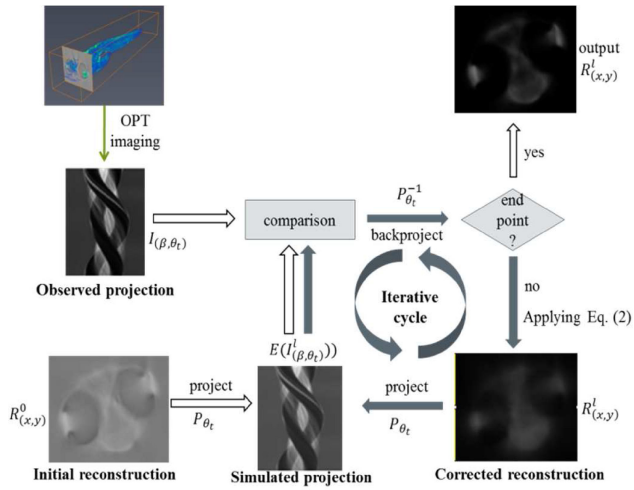

Fig. 2. Workflow of iterative reconstruction in OPT. Example is given on a zebrafish larvae of 6 days post fertilization (dpf).

of quantitative evaluation on reconstruction in OPT. This disadvantage is caused by the lack of benchmarks for samples. In this particular situation, the formulation of an alternative evaluation method according to the specific research problem is considered to be feasible and applicable. With this idea we transfer the evaluation of reconstruction to that of segmentation which can be easily obtained from the reconstruction data; in our experiments these are zebrafish larvae and juveniles. The rationale of the transfer originates from the fact that we are expecting better segmentation results from different reconstructions on the same tomogram data. Therefore, this transfer is considered valid under the assumption that with the same segmentation algorithm a better segmentation result arises from a better reconstruction output. By changing the evaluation from reconstruction to segmentation, we are able to find better parameters for reconstruction in an objective manner. This can be considered as an optimization of iterative reconstruction.

Iterative reconstruction and segmentation are both known techniques, there is, however, as far as known to us, no previous research that uses segmentation for optimization of the reconstruction. In this paper, we explore how and to what extent segmentation is able to contribute to the iterative reconstruction in OPT, with the focus on the parameter optimization for iterative reconstruction so as to improve its reconstruction performance. The remainder of this paper is structured as follows. In Section II the process of iterative reconstruction will be briefly introduced. In Section III, we will focus on the explanation of parameter optimization. In Section IV, the specific schema and approach for parameter optimization will be exhaustively discussed. In Section V the experimental results are presented and discussed. Finally, in Section V we present our conclusions, raise some limitations and suggest future work.

II. Iterative Reconstruction for OPT

In general, iterative reconstruction can result in a more accurate OPT 3D image than a reconstruction obtained using FBP [4]. In Fig. 2 the workflow of iterative reconstruction is depicted as

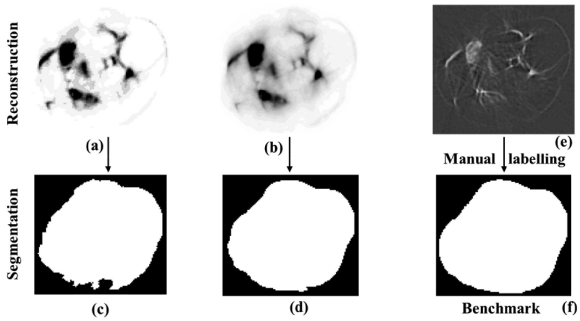

Fig. 3. An example showing the effect of reconstruction parameters on segmentation performance. (a) and (b) The slices reconstructed from two different parameters. (c) and (d) The corresponding segmentation results. (f) The segmentation benchmark for comparison, which was manually segmented from FBP reconstruction, with (e) showing the inverted bright-field image slice we used for the labeling.

applied to a typical zebrafish sample on a slice by slice basis. The observed projections are acquired from the OPT imaging system and are here defined as the sinogram $I_{(\beta,\theta_t)}$. By using the ordered subset expectation maximization (OSEM) algorithm [20], [18], [21], the reconstructed slice $R^l_{(x,y)}$is updated based on the differences between the observed projection and the simulated projection in reconstruction space using Eq. (1), with an initial reconstruction slice $R^0_{(x,y)}$. The simulated projection is updated as $E(I^l_{(\beta,\theta_t)}) = (P_{\theta_t} R^l_{(x,y)})$ and $E(I^0_{(\beta,\theta_t)}) = P_{\theta_t} R^0_{(x,y)}$ for the first update. This difference $I_{(\beta,\theta_t)} / E(I^l_{(\beta,\theta_t)})$ in projection space is reconstructed to 3D image space using back projection $P^{-1}_{\theta_t}$, which is finally used for updating the slice $R^l_{(x,y)}$ as shown in Eq. (1). As we can see from Fig. 2, in the iterative framework both the endpoint and the initial reconstruction $R^0_{(x,y)}$ play an important role in the final results, which will be studied in the following sections.

$$R^{l+1}_{(x,y)} = R^l_{(x,y)} \frac{\sum_{\theta_t \in I_t} (P_{(\beta,\theta_t)} I_{(\beta,\theta_t)} / (P_{(\beta,\theta_t)} R^l_{(x,y)}))}{\sum_{\theta_t \in I_t} P_{(\beta,\theta_t)}} \quad (1)$$

III. Parameter Optimization for Iterative Reconstruction

Parameters for iterative reconstruction can be optimized based on the performance assessed on reconstructed results. Nevertheless, due to the lack of benchmarks for direct reconstruction evaluation in OPT we consider the assessment according to the segmentation performance of the 3D images reconstructed with different parameters. To this end, the framework of this idea will be elaborated first. This framework is proposed under the assumption that the segmentation method is able to learn the discontinuity in intensities of the images of our dataset. In order to guarantee this, we employ a convolutional neural network (CNN) which is known for its excellent performance in image segmentation.

A. Impact of Reconstruction Parameter on Segmentation

In Fig. 3, an example slice (head part) of a 25 *dpf* zebrafish is given, explaining how different reconstruction parameters influence the segmentation performance. Fig. 3(a) and (b) are two slices reconstructed from the same iterative reconstruction algorithm using different parameters. Fig. 3(c) and (d) show the corresponding segmentation results based on the reconstructed slices of (a) and (b). The segmentation benchmark of this slice is displayed in (f), which is obtained from a manual segmentation of the FBP reconstruction (e). Here the different constituents are comprehensively presented in the image, i.e., both clearer contour and artefacts. When visually comparing the reconstructed slices and the segmentation performance, we observe that different reconstruction parameters will produce different slices in the 3D image. This will, consequently, result in distinctly different segmentation results. For instance, the slice in (b) has better segmentation performance, as shown in (d), compared to the performance (c) from the slice in (a). With this assumption, we can optimize the parameters based on the segmentation performance of the slices of the 3D image that are reconstructed with different parameters.

B. Parameter Optimization Framework

The framework of parameter optimization for iterative reconstruction integrates the reconstruction and segmentation process as a whole (cf. Fig. 4). In OPT a tomogram is referred to as $I_{(z,\beta,\theta)}$, with z and β representing the pixel position of tomogram at the projection angle θ. The 3D image is obtained by implementing the iterative reconstruction algorithm $f_{\boldsymbol{\alpha_n}}$ on the tomograms as $R^{\boldsymbol{\alpha_n}}_{(x,y,z)} = f_{\boldsymbol{\alpha_n}}(I_{(z,\beta,\theta)})$ with $\alpha_{\boldsymbol{n}}$ being the parameters required for iterative reconstruction. For the same tomogram set $I_{(z,\beta,\theta)}$ it is assumed that there are *N* reconstructed 3D image groups $\{R^{\alpha_1}_{(x,y,z)}, \ldots, R^{\alpha_N}_{(x,y,z)}\}$ produced from iterative reconstruction functions $\{f_{\alpha_1}, \ldots, f_{\alpha_N}\}$ with $\{\alpha_1, \ldots, \alpha_N\}$ representing the variation of parameters.

The results from the reconstructions can further be segmented according to a specific criterion for the given data set, achieving the segmentation result $S^{\boldsymbol{\alpha_n}}_{(x,y,z)}$, where $S^{\boldsymbol{\alpha_n}}_{(x,y,z)} = g_{\boldsymbol{\alpha_n}}(R^{\boldsymbol{\alpha_n}}_{(x,y,z)})$. Therefore, the segmentation result can be formulated as:

$$S^{\boldsymbol{\alpha_n}}_{(x,y,z)} = g_{\boldsymbol{\alpha_n}} \left[f_{\boldsymbol{\alpha_n}} \left(I_{(x_\theta, y_\theta, \theta)} \right) \right] \quad (2)$$

With $g_{\boldsymbol{\alpha_n}}$ indicating the segmentation function trained with the 2D U-net [22] CNN on the 3D image group reconstructed with parameterα_n. This means that, given the same tomogram, training the segmentation network with the 3D image reconstructed from different parameters will produce different network outputs for segmentation. From this notion, the optimization of reconstruction parameter can be approximately transferred to a search for a better $\alpha_n$that produces a 3D image with a better segmentation. This is under the assumption that the benchmark of the segmentation is known. Therefore, we need a ground truth segmentation of the zebrafish model as used in our experiments.

By evaluating the *N* 3D image groups based on their segmentation performance, we can achieve the best reconstruction parameters ranging from α_1 to α_N. If there are *K* samples for reconstruction and segmentation, then in each reconstruction group we have $R^{\boldsymbol{\alpha_n}}_{(x,y,z)} = \{R^{\boldsymbol{\alpha_n}}_{1(x,y,z)}, \ldots, R^{\boldsymbol{\alpha_n}}_{k(x,y,z)}, \ldots, R^{\boldsymbol{\alpha_n}}_{K(x,y,z)}\}$

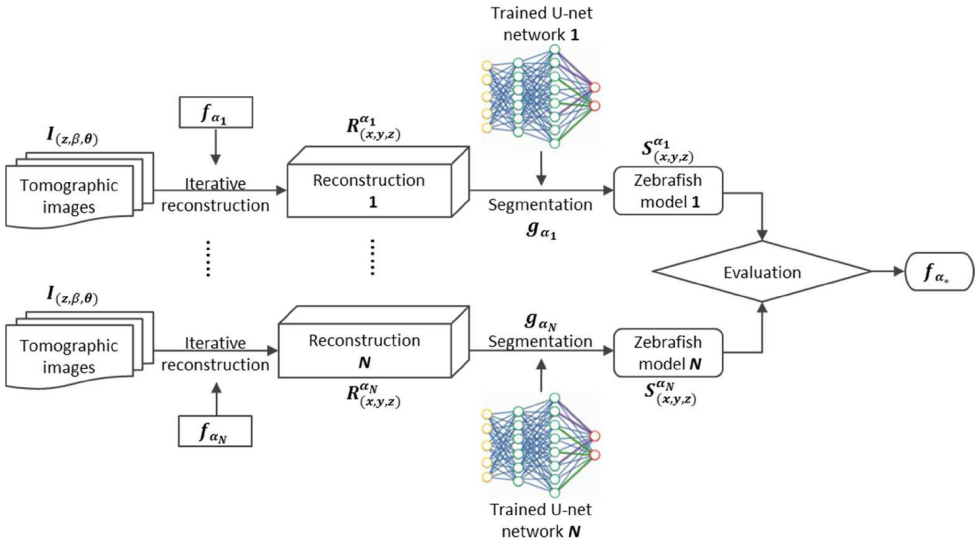

Fig. 4. The framework for parameter optimization for iterative reconstruction based on the corresponding segmentation performance. The 2D U-net [22] CNN is applied to train the segmentation model within each parameter group.

and in each segmentation group we have $S^{\boldsymbol{\alpha_n}}_{(x,y,z)} = \{S^{\boldsymbol{\alpha_n}}_{1(x,y,z)}, \ldots, S^{\boldsymbol{\alpha_n}}_{k(x,y,z)}, \ldots, S^{\boldsymbol{\alpha_n}}_{K(x,y,z)}\}$. It is worth mentioning that the segmentation network in each parameter group is trained and evaluated independently on each dataset, because from an experimental perspective it is considered valuable to minimize the correlation between groups in both the reconstruction and the segmentation process. With the employed U-net CNN [22] configured with the same hyper-parameter configuration, N segmentation networks $\{g_{\boldsymbol{\alpha}_1}, \ldots, g_{\boldsymbol{\alpha_n}} \ldots, g_{\boldsymbol{\alpha}_N}\}$ are independently trained, corresponding to N reconstruction groups. Even though each individual network may have a different segmentation performance from the others, with the same hyper-parameter configuration it is thought the differences mainly result from the differentiation of the training data from different reconstruction groups.

By testing or evaluating the segmentation performance independently on each group of reconstruction data, we can identify the group that performed best and accordingly find the optimal reconstruction parameter $f_{\boldsymbol{\alpha}_*}$. In the OSEM iterative reconstruction algorithm there are several parameters required, but we focus on the two parameters: iteration number (η) and initial reconstruction (γ). The different combinations of η and γ comprise $\{\alpha_1, \ldots, \alpha_n, \ldots, \alpha_N\}$, meaning that if $\eta = \{\eta_1, \ldots, \eta_i, \ldots, \eta_p\}$ and $\gamma = \{\gamma_1, \ldots, \gamma_j, \ldots, \gamma_q\}$, then $\alpha_n = (\eta_i, \ \gamma_j)$ and $N = p \cdot q$.

IV. Implementation for Parameter Assessment Using Segmentation

A. Segmentation Approach

As for our data, the zebrafish samples are transparent which often results in a somewhat discontinuous object contour in the 3D bright-field image. When the intensities in the foreground and the background are very similar, traditional segmentation approaches are very much challenged for a good result. This is in particular the case for discontinuities in the outline (contour) of the object in the image space [23]. Different from traditional segmentation methods, a CNN can, however, learn the structural and contextual information in different scales. With this approach our research questions can be addressed well. We define our segmentation task as a binary segmentation on transparent samples in intensity image space. This means that, for our problem, a small network such as 2D U-net [22] is preferred over a more complex network.

The segmentation network for zebrafish in each α_n-specified 3D image group is independently trained and tested. The number of segmentation networks for the parameter optimization framework is dependent on the parameter combination, as $N = p \cdot q$ for two parameters in our case.

Within each group $R^{\alpha_n}_{(x,y,z)}$, the 2D U-net segmentation network [22] takes the reconstructed slices as input. As the output layer, the map activated by a Sigmoid function [24], reflects the response to the zebrafish segmentation ranging from 0 to 1. The segmentation mask is obtained when implementing a threshold on the map. Different from the work in [22], we employ the simplest binary cross entropy [25] as the loss function without considering the weight of each pixel in the image. The network is trained with the Adam optimizer [26] implemented in Keras [27], with 500 epochs being set for all the networks.

1) Data Split: For a specific group $R^{\alpha_n}_{(x,y,z)}$, a certain, typically small, ratio of reconstructed slices from the 3D images are sampled at regular intervals for training while the rest, the larger part, is used for testing. The rationale for training on a small rather than large ratio of data lies in the fact of information redundancy among adjacent slices in 3D space. Moreover, this will, to a large extent, reduce the workload of manual labeling. To further decrease the labeling workload, an interpolation approach is applied. The tool for interpolation labeling is available in the software [28] and the results can be further manually verified. The 3D images from the FBP reconstruction are used for labeling because of its capacity of presenting comprehensive information

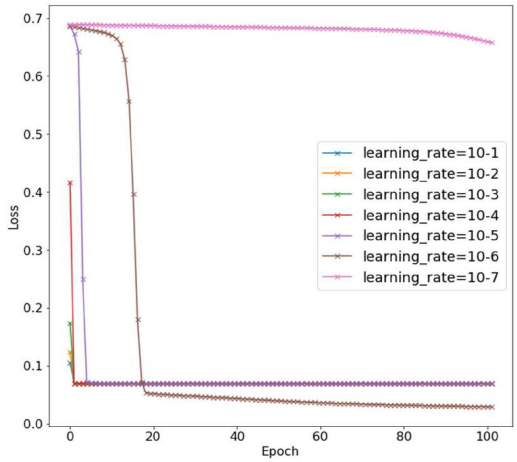

Fig. 5. The profiles of the decay loss for different learning rates in 100 epochs. The learning rates observed are from 10^{-1} to 10^{-7}.

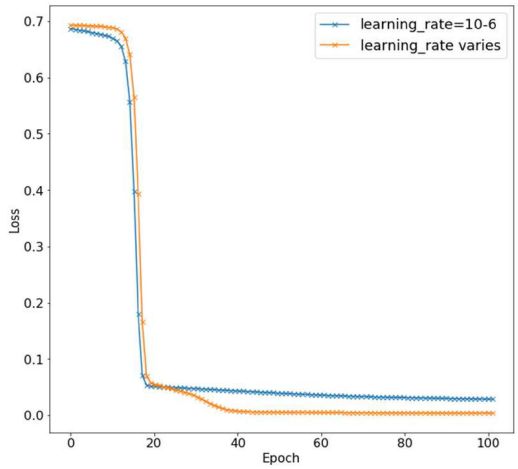

Fig. 6. The comparison of the decay loss between learning rate 10^{-6} and the proposed learning rate schema in 100 epochs. The proposed learning rate increases from 10^{-6} to 10^{-4}.

on the object in the image. Details of the data properties used for the experiments will be further elaborated in the experimental section.

2) Learning Rate: On our data, we observe the impact of different learning rates on the training loss. This is shown in Fig. 5, where loss curves for decreasing learning rates are plotted. As the learning rate increases, the learning process quickly drops to a local minimum. This should be avoided and therefore we propose another learning schema. To prevent dropping to a local minimum, at the onset of the training process a smaller learning rate is required while a relatively higher learning rate is needed to avoid the computational cost of an extremely slow convergence later on in the training process. To meet these requirements, the learning rate schema is designed as:

$$lr^{(i+1)_e} = lr^{i_e} \cdot \lambda^{1+N_{i_e}} \tag{3}$$

where $lr^{(i+1)_e}$ and lr^{i_e} represent the learning rate at the i^{th} and $(i+1)^{\text{th}}$ effective epoch respectively. An epoch is considered to be effective only when it decreases the loss function. For an effective epoch, the learning rate will be used for the next update so as to increase the learning rate, while the learning rate of an ineffective epoch will be propagated to the next epoch. In Eq. (3), N_{i_e} counts the effective epochs and λ indicates the base of the exponential function which is close to but greater than 1; for our experiments set to 1.001. The initial learning rate is set as 1e-6 and the upper limit is set as 1e-4 in order to avoid divergence as the learning rate increases.

In Fig. 6 the profiles for loss decrease between the fixed learning rate (1e-6) and the proposed learning rate, are compared. It is observed that the proposed schema starts from a point in the network which has a larger loss, but as the learning rate slowly increases the loss decreases, thereby avoiding the local minimum. However, as the number of epochs increases, the loss rapidly drops and reaches a smaller level which a fixed learning rate of 10^{-6} otherwise fails to obtain.

The segmentation describes the process of implementing the trained network on the k^{th} test voxel $R^{\alpha_n}_{k(x,y,z)}$. With the 2D kernel for training the segmentation network, it shows limited ability to consider the relationship between slices. It is assumed that the segmentation from network $g_{\boldsymbol{\alpha_n}}$ is indicated as $M^{\alpha_n}_{(x,y,z)} \in \{0,\ 1\}$, a binary map corresponding to the testing voxel. Considering the correlation between adjacent slice, a refining post-processing procedure is introduced as follows. If $M^{\alpha_n}_{(x,y,z)} \oplus M^{\alpha_n}_{(x,y,z-1)} = 1$ and $M^{\alpha_n}_{(x,y,z)} \oplus M^{\alpha_n}_{(x,y,z+1)} = 1$, then $M^{\alpha_n}_{(x,y,z)}$ is set to equal to $M^{\alpha_n}_{(x,y,z-1)}$ and $M^{\alpha_n}_{(x,y,z+1)}$. This process particularly works for the correcting of the isolated segmentation error in *Z* direction. The segmentation result after the refined process is referred to as $S^{\alpha_n}_{(x,y,z)}$.

B. Evaluation Criterion

The evaluation component as depicted in Fig. 4 is accomplished by figuring out the group which has the best segmentation performance using the independently trained network, given the 3D zebrafish data and *N* different parameter groups $\{\alpha_1, \ldots, \alpha_N\}$. Different from 2D image segmentation, evaluation of image segmentation in 3D should be implemented based on a 3D image with the slices being well ordered. This means that each 3D sample should be independently evaluated, rather than evaluating all the slices in 2D across samples. Taking this into account the objective function for optimization of reconstruction parameters α is formulated as follows:

$$\alpha^* = \min_{\alpha} \frac{1}{K} \sum_{k=1}^{K} MCC\left(S^{\boldsymbol{\alpha}}_{k(\boldsymbol{x},\boldsymbol{y},\boldsymbol{z})}\right) \tag{4}$$

where *K* is the number of samples used for evaluation. For each sample, i.e., a 3D image of a zebrafish, the overall segmentation performance in 3D is measured with Matthew's correlation coefficient (MCC) [29], thereby excluding the training slices from our experiments. This coefficient takes into account true and false positives and negatives. Moreover, it is generally regarded as a balanced measure for classes of very different sizes. This characteristic matches well with the measurement requirements in these experiments. The aim of the parameter optimization is

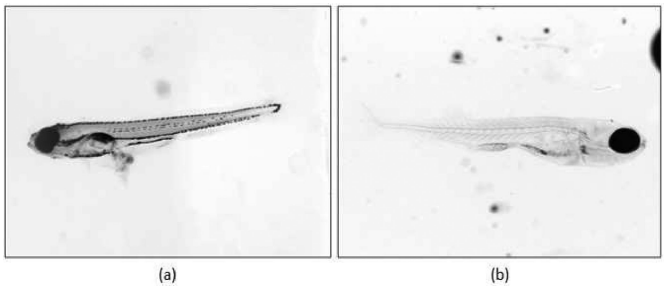

Fig. 7. Samples of zebrafish with different preparation protocols in the bright-field mode. (a) One example of a tomogram for the 5 dpf zebrafish clearing with BABB protocol [30]. (b) One example of tomogram for the 25 dpf zebrafish cleared with CUBIC protocol [31].

TABLE I
SEGMENTATION PERFORMANCES OF ITERATIVE RECONSTRUCTIONS IMPLEMENTED WITH VARIOUS ITERATION NUMBERS AND NO-INITIAL RECONSTRUCTION ON THE THREE 5 *DPF* ZEBRAFISH

No-initial	Fish1 (%)	Fish2 (%)	Fish3 (%)	Average (%)
5-iteration	98.22	97.94	97.87	98.01
10-iteration	**98.23**	**98.13**	**97.93**	**98.10**
15-iteration	97.53	97.37	97.25	97.38
20-iteration	97.34	97.10	96.90	97.11
25-iteration	97.73	97.69	97.68	97.70

to find the optimal parameter group α^* which produces the 3D images that has a maximum overall segmentation performance.

V. EXPERIMENTS

In this section, we study the parameter optimization for iterative reconstruction, experimenting on two zebrafish datasets that were prepared with different protocols for clearing. Sample clearing is of importance to increase sample transparency and internal object visibility in OPT (e.g., fluorescently labeled organ or tumor). Benzyl alcohol benzyl benzoate (BABB) treatment is standard for clearing, but can result in an undesirable loss of fluorescence [30]. An alternative treatment is the N,N,N,N-tetrakis (2-hydroxypropyl) ethylenediamine-based unobstructed brain imaging cocktails and computational analysis (CUBIC) approach, which retains fluorescence but takes a duration longer for clearing [31].

A. Datasets and Experimental Settings

In order to implement the experiments for parameter optimization, six zebrafish are used for OPT imaging. They are split into two groups and have been prepared with different protocols which result in different contrast and intensity distributions. Fig. 7 shows two example images of zebrafish from the bright-field mode of our OPT system. These two samples correspond to two different protocols for sample preparation. The motivation for using bright-field rather than fluorescence is given by the fact that in zebrafish imaging, bright-field images provide a clear outline information of a sample. This will provide more prior knowledge to benchmark for segmentation. Fig. 7(a) corresponds to the tomogram of 5 *dpf* cleared zebrafish with BABB protocol [30], while (b) displays the 25 *dpf* zebrafish with CUBIC protocol [31]. In the bright-field mode, we can easily observe the difference of intensity distribution between them.

For each preparation protocol or dataset, there are three zebrafish studied for parameter optimization. Each reconstructed sample, i.e., a 3D zebrafish image, consists of 1360 slices produced from a set of 400 tomogram images using the reconstruction algorithm. This compromises to 4080 slices with an image size of 512×512 for each group or experiment implementation. To obtain the segmentation network all the zebrafish slices within each group are evenly distributed into the training set of 20% with a validation rate of 10% and test set of 80%. The ground-truth segmentations are labeled based on the FBP results. The segmentation performance of each group consists of average the MCC scores [29] of all samples on its test slices as depicted in the evaluation criterion section.

B. Parameter Optimization

The two parameters, i.e., iteration number η and initial reconstruction γ, are studied. First, for each dataset the effect of iteration number on segmentation performance is investigated. To this end, five groups of 3D images reconstructed from different iteration numbers are generated, combing the cost of computation and effectiveness of the reconstruction. Each group corresponds to one of the five iteration numbers, i.e., $\eta = \{5,\ 10,\ 15,\ 20, 25\}$ with $=\ 5$. We consider 5 to be a reasonable step size for the assessment of reconstruction performances based on different numbers of iteration.

The iteration number η is optimized by comparing the segmentation performance of each group. For initial reconstruction γ we compare the performance with an initial 3D image from the FBP results (referred to as FBP-initial) and a same shape 3D image initialized by 1 (referred to as No-initial), with $q\ =\ 2$. Therefore, there are $N\ =\ p \cdot q\ =\ 10$ groups of algorithmic parameters for optimization on each dataset.

1) Experiments on 5 dpf Zebrafish: The first data used in the experiments are three 5 *dpf* zebrafish prepared with the BABB protocol [30]. The MCC performance on the test dataset of each group and the individual samples are presented in Table I and Table II. The two tables show the performance differences of different initial reconstruction settings, with Table I presenting the results with the No-initial reconstruction setting while Table II corresponding to the FBP-initial results. Results are obtained based on the same training configuration of segmentation network.

For each sample with a particular iteration number, the performance represents the overall 3D MCC score of segmentation performance on the test slices. Such as in Table I for Fish1 with 5-iteration, the segmentation performance of Fish1 in 3D is 98.22%. The results of the highest segmentation performance for

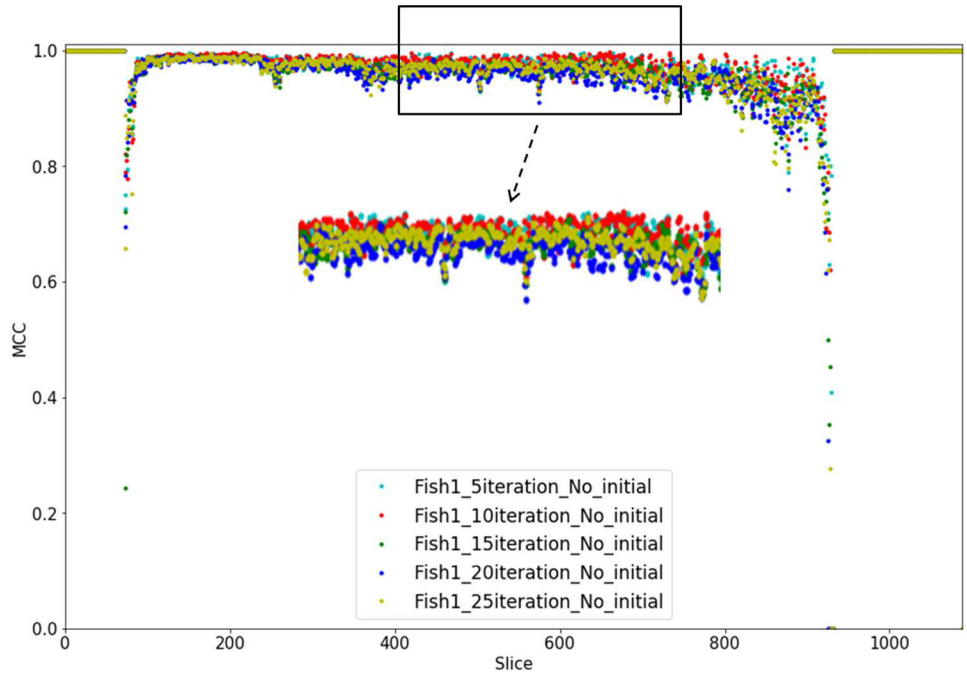

Fig. 8. Segmentation performance of reconstructed slices with different iteration numbers in a No-initial setting on the 5 dpf Fish1. Each point represents the MCC score of each test slice of the 3D image for segmentation. The rectangular area is zoomed.

TABLE II
SEGMENTATION PERFORMANCES OF ITERATIVE RECONSTRUCTIONS IMPLEMENTED WITH VARIOUS ITERATION NUMBERS AND FBP-INITIAL RECONSTRUCTION ON THE THREE 5 *DPF* ZEBRAFISH

FBP-initial	Fish1 (%)	Fish2 (%)	Fish3 (%)	Average (%)
5-iteration	98.28	98.00	97.95	98.08
10-iteration	**98.38**	98.27	**98.17**	**98.27**
15-iteration	98.29	98.13	98.05	98.16
20-iteration	98.34	98.04	97.94	98.11
25-iteration	98.30	**98.33**	98.02	98.22

each sample across the different iteration numbers are emphasized in bold face. From the results obtained from the 3 zebrafish, it is observed that 10-iteration achieves the best performance for both No-initial and FBP-initial reconstruction. Even though in Table II the 25-iteration reconstruction outperforms that of the 10-iteration on Fish2 with the FBP-initial setting, the difference is in fact very small, whilst the 10-iteration far outperforms other iteration numbers in most cases. Regarding the different initial schemas, the FBP-initial method outperforms the No-initial approach in terms of segmentation results on the three zebrafish samples with the same iteration number setting.

Table I and Table II present quantitative measures for segmentation performance on the 3D images. However, this does not provide performance details of each slice inside of the 3D volume. In order to achieve these segmentation performances for all slices within each sample, each individual 3D image needs to be investigated. Figures 8 and 9 provide an example for that on zebrafish sample 1. Slices from the left to the right correspond to the zebrafish from the head to the tail. Each point in Figures 8 and 9 stands for an MCC score of a slice. The MCC score of each slice ranges from 0 to 1. The value of 1.0 on the left and right side of the figures implies a background slice in the reconstructed 3D data. Close to the background slices are the critical slices which are indistinguishable for segmentation. That is why they have quite low MCC score performances on both sides of the 3D data, i.e., the critical slices between the head or tail and background.

By comparing the distribution of MCCs on all slices in Fig. 8, we can also see that the 3D image group with 10-iteration has more points with larger MCC and less with smaller MCC, compared to other groups. Similar results can be observed in Fig. 9 for FBP-initial reconstruction, even though it is not as distinct as the results in Fig. 8. The comparisons of segmentation performance on the 5 *dpf* zebrafish reconstructed with different iterations, both for No-initial and FBP-initial, indicate that the reconstruction with the 10-iteration produces the most desirable results.

2) Experiments on 25 dpf Zebrafish: As far as the variation of data distribution and experimental environment are concerned, three 25 *dpf* zebrafish cleared with CUBIC protocol [31] are also used for experiments. The segmentation performances of test data on each sample and in each 3D image group are demonstrated in Tables III and IV, with the average MCC corresponding to the segmentation performance of each group while MCC showing the performance of each sample. As with Table I and Table II, the best performance of individual sample and group are set in bold face. Overall, the segmentation performance indicates that the FBP-initial reconstruction method outperforms the No-initial approach. Furthermore, in both cases, according to the MCC performance, 10-iteration gives the best performance,

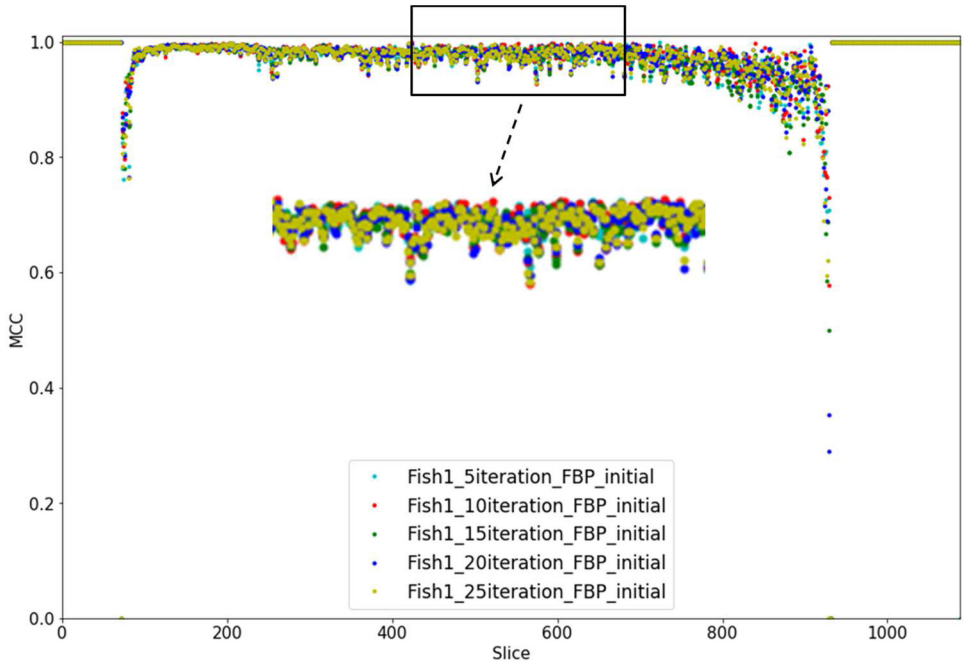

Fig. 9. Segmentation performance of reconstructed slices with different iteration numbers in a FBP-initial setting on the 5 dpf Fish1. Each point represents the MCC score of each test slice of the 3D image for segmentation. The rectangular area is zoomed.

TABLE III
SEGMENTATION PERFORMANCES OF ITERATIVE RECONSTRUCTIONS IMPLEMENTED WITH VARIOUS ITERATION NUMBERS AND NO-INITIAL RECONSTRUCTION ON THE THREE 25 *DPF* ZEBRAFISH

No-initial	Fish1 (%)	Fish2 (%)	Fish3 (%)	Average (%)
5-iteration	97.78	96.47	97.71	97.32
10-iteration	**97.95**	**96.69**	97.82	**97.49**
15-iteration	97.84	95.13	**97.88**	96.95
20-iteration	97.83	86.08	97.81	93.90
25-iteration	97.34	77.21	96.97	90.51

TABLE IV
SEGMENTATION PERFORMANCES OF ITERATIVE RECONSTRUCTIONS IMPLEMENTED WITH VARIOUS ITERATION NUMBERS AND FBP-INITIAL RECONSTRUCTION ON THE THREE 25 *DPF* ZEBRAFISH

FBP-initial	Fish1 (%)	Fish2 (%)	Fish3 (%)	Average (%)
5-iteration	98.05	**97.18**	98.16	97.80
10-iteration	**98.27**	97.15	**98.37**	**97.93**
15-iteration	97.68	94.11	97.46	96.42
20-iteration	97.88	91.54	98.00	95.81
25-iteration	97.88	83.82	97.83	93.18

even though occasionally the other iteration numbers outperform the 10-iteration with minor differences. This is consistent with the observations obtained with the 5*dpf* zebrafish.

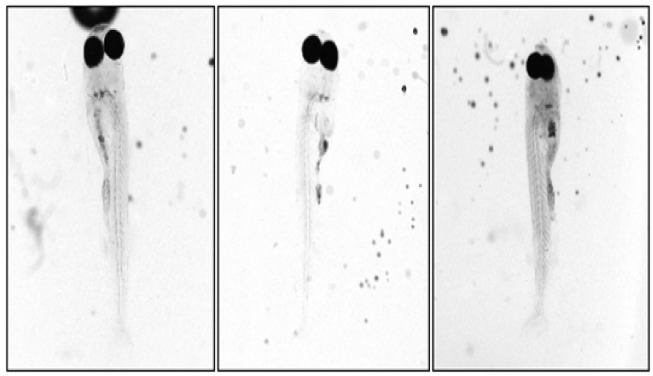

Fig. 10. The tomogram of the 25 dpf Fish1, Fish2 and Fish3. They are shown in mounting orientation in the OPT imaging system. Fish2 has a lower contrast than the other two, with comparable background noise.

However, compared to the 5 *dpf* zebrafish, segmentation performance on the 25 *dpf* zebrafish is, in general, a bit lower and there is a larger deviation across the 3D image groups. For example, if we compare Fish1 of both datasets in the No-initial case (in Table I and Table III), then Fish1 of 5 *dpf* zebrafish as shown in Fig. 7(a), has a MCC range of [97.34, 98.23] outperforming the range of [97.34, 97.95] for Fish1 of 25 *dpf* zebrafish in Fig. 7(b). Similar comparisons between the two datasets, corresponding to the two protocols, can be made for the other samples. In general, we conclude that the CUBIC clearing protocol makes the zebrafish more transparent for OPT imaging compared to the BABB protocol. We need to acknowledge that a higher transparency of sample results in a higher uniformity within the sample henceforth a lower contrast between the foreground (zebrafish) and background tomograms in the 3D

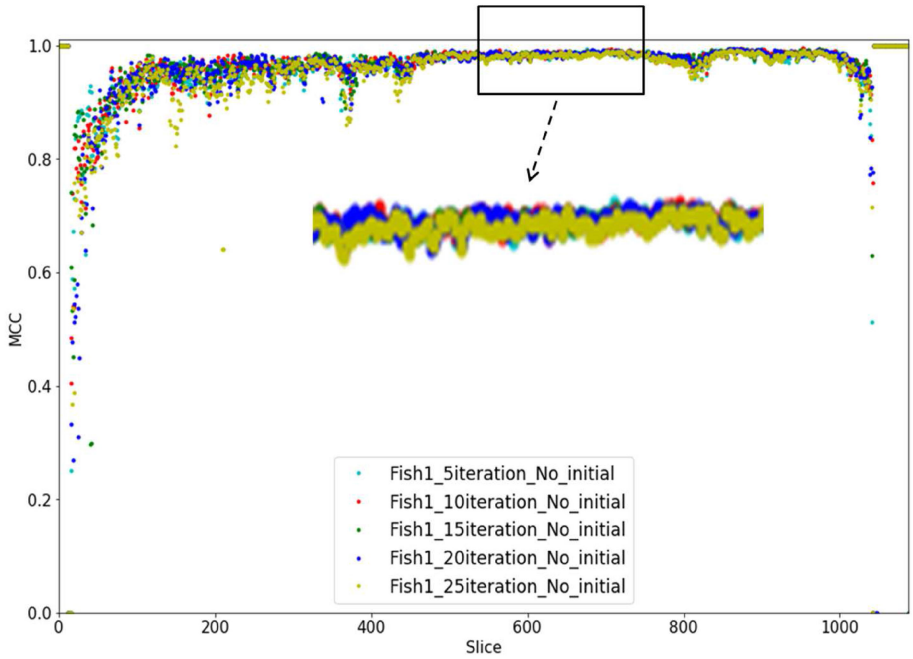

Fig. 11. Segmentation performance of reconstructed slices with different iteration numbers in a No-initial setting on the 25 dpf Fish1. The performance is represented by MCC score of each test slice of the 3D image. The rectangular area is zoomed.

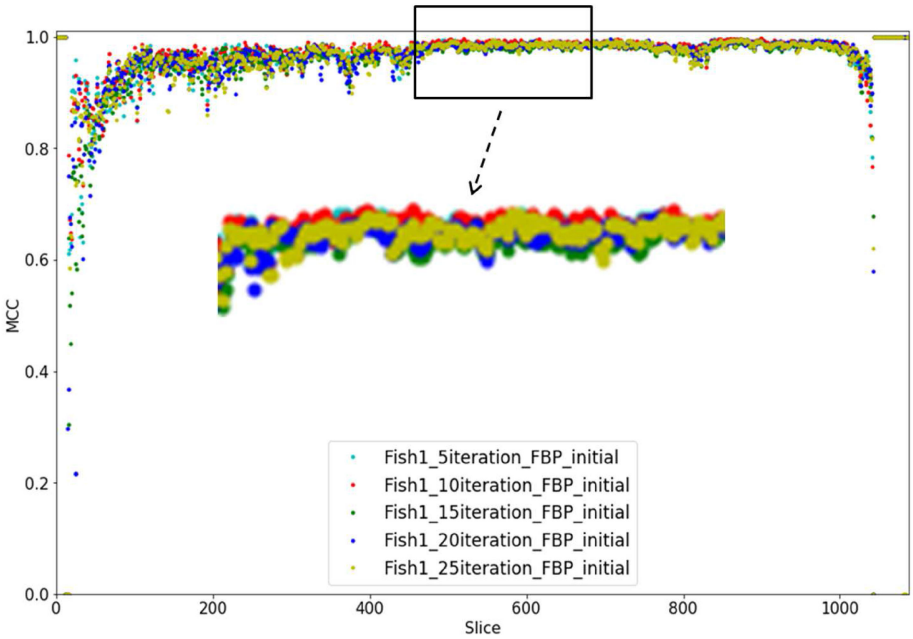

Fig. 12. Segmentation performance of reconstructed slices with different iteration numbers in a FBP-initial setting on the 25 dpf Fish1. The performance is represented by MCC score of each test slice of the 3D image. The rectangular area is zoomed.

images, particularly at the edge of the object/sample. Such 3D image will consequently have a lower segmentation performance and will be more sensitive to the number of iterations in the process of reconstruction.

In Table III and Table IV we can readily see that as iteration number increases the performance of sample Fish2 decreases dramatically whilst sample Fish1 and Fish3 decrease much less. This is because sample Fish2 is of lower contrast due to a higher transparency of the sample; this can be seen in Fig. 10. When the iteration number increases the information loss of the zebrafish body in the reconstruction is much more obvious. This makes it more difficult to be correctly segmented.

Regarding the performance of individual slices within the 25 *dpf* Fish1 for both No-initial and FBP-initial configuration, they are separately shown in Figures 11 and 12. For both cases, 10-iteration reconstruction outperforms other groups from either 2D slice or 3D volume scale.

C. Discussion

In this section an overall discussion on the experiments is presented. In the experimental section, we focus on the study of parameter optimization for the iterative reconstruction concerning its performance potential for OPT reconstruction as shown in Fig. 1. This means that the effect of different reconstruction parameters needs to be investigated. This is accomplished by studying the two parameters, i.e., the number of iteration and the initialization of reconstruction. We applied this in experiments with two zebrafish datasets, each with a different image intensity distribution. According to these experiments, the combination of 10-iteration and FBP-initialization has proven to produce the most desirable and preferable 3D image, compared to the other combinations. Additionally, 10-iteration is also acceptable for reconstruction implementation with respect to the computational cost. When comparing the segmentation performance across datasets, we find that the contrast rich dataset performs better, which can be understood from a theoretical perspective. Because a very transparent sample produces an intensity distribution which critically distinguishes the object in both the tomogram and 3D image in OPT. This, therefore, brings about more complications for the segmentation.

In order to guarantee good performance of the segmentation with the CNN, a different learning schema was necessary. The research on this learning schema was included in our experiments (cf. Section IV). We have shown that with our learning schema a stagnation in a local minimum is prevented. In addition to the learning rate curves we tested on the validation loss. For the different learning rates, the curve for validation loss is in line with that of the training loss. Although the size of the set was relatively small, yet there was no over-fitting in the data which is confirmed by the results on the test data set as presented in Tables I–IV. The schema provides us with a good performance of the segmentation. This performance subsequently supports the assessment of the iterative reconstruction by showing a better performance with a certain parameter set. As aforementioned the trend for an optimal parameter setting is demonstrated as 10-interation with FBP initial.

In this work the experiments are conducted on a finite number of zebrafish samples. With the current trend of high-throughput analysis on zebrafish, in the near future an increase in the samples size will be considered to further confirm the trends that we have established in our experiments.

VI. Conclusion

The research presented in this paper is the application of an iterative reconstruction algorithm, specifically OSEM [20], and the exploration of approaches to optimize the reconstruction parameters for that algorithm. The OSEM algorithm produces superior 3D images in comparison with the FBP algorithm in terms of streak artefact elimination that otherwise occur when the signals in OPT tomograms are very dense. The method for improvement of the reconstruction consists of optimizing the parameters for the OSEM algorithm, which requires the evaluation of reconstructed 3D images. As we are restricted by the lack of benchmarks for OPT reconstruction imaging, we have used an alternative approach that is conducted by the evaluation of the segmentation of the resulting 3D reconstruction. The integration of segmentation evaluation into parameter optimization for iterative reconstruction may not result in overall optimal parameters for all cases. But, to the best of our knowledge, it provides a good and reasonable way for guaranteeing an optimized reconstruction result, whilst taking into consideration both the reconstruction quality and computational cost. From our results the trend for the parameters is clear and it will allow us to apply these on a larger scale on similar samples. It is worth to point out that even though OSEM produces promising results for highly transparent samples, such as our 25 *dpf* Fish2 with 10-iteration, it could also be possible that a sample is simply too transparent to produce any significant reconstruction results with the same OSEM parameters. In such an extreme case, decreasing the iteration number might help recover more information in combination with an image blur [7], [32].

The method presented here can be utilized to reconstruct and quantify fluorescently labeled structures, for example tumor in the zebrafish as disease model for neuroblastoma [33]. Quantification of tumor volume and changes therein upon drug treatment will characterize efficacy of newly screened drugs. By linking the drug effect to its internal exposure, for which recently methods have been established in the zebrafish [34]–[36], the drug exposure-response relationship can be established, which is the cornerstone for translation of drug effects across species, towards the clinic.

Acknowledgment

The authors would like to express their gratitude to Shuning He (Dana-Farber Cancer Institute, Boston, USA) for making available the fixed 25 dpf zebrafish samples. All 5 dpf zebrafish husbandry and experiments complied with European regulation [37]. All 25 dpf zebrafish husbandry and experiments were in accordance with Dana-Farber Cancer Institute IACUC-approved protocol #02–107.

References

[1] R. C. van Wijk, E. H. J. Krekels, T. Hankemeier, H. P. Spaink, and P. H. van der Graaf, "Systems pharmacology of hepatic metabolism in zebrafish larvae," *Drug Discov. Today: Dis. Models*, vol. 22, pp. 27–34, 2016.

[2] P. Schulthess, R. C. Van Wijk, E. H. J. Krekels, J. W. T. Yates, H. P. Spaink, and P. H. Van Der Graaf, "Outside-in systems pharmacology combines innovative computational methods with high-throughput whole vertebrate studies," *CPT Pharmacometrics & Syst. Pharmacol.*, vol. 7, no. 5, pp. 285–287, 2018.

[3] J. R. Walls, J. G. Sled, J. Sharpe, and R. M. Henkelman, "Correction of artefacts in optical projection tomography," *Phys. Med. Biol.*, vol. 50, no. 19, pp. 4645–4665, 2005.

[4] D. E. Dudgeon and R. M. Mersereau, "Multidimensional digital signal processing," *IEEE Commun. Mag.*, vol. 78, no. 4, pp. 590–597, Apr. 1990.

[5] J. B. Pawley, *Handbook Biological Confocal Microscopy*, Springer Science & Business Media, vol. 236, 2006.

[6] A. Nwaneshiudu, C. Kuschal, F. H. Sakamoto, R. Rox Anderson, K. Schwarzenberger, and R. C. Young, "Introduction to confocal microscopy," *J. Invest. Dermatol.*, vol. 132, no. 12, pp. 1–5, 2012.

[7] X. Tang, G. E. M. Lamers, and F. J. Verbeek, "3D image deblur using point spread function modelling for optical projection tomography," in *Proc. BIOIMAGING 2019 - 6th Int. Conf. Bioimaging, Proc.; Part 12th Int. Joint Conf. Biomed. Eng. Syst. Technol., BIOSTEC*, 2019, pp. 67–75.

[8] L. L. Geyer *et al.*, "State of the art: Iterative CT reconstruction techniques," *Radiology*, vol. 276, no. 2, pp. 339–357, 2015.
[9] D. Hahn *et al.*, "Statistical iterative reconstruction algorithm for X-ray phase-contrast cT," *Sci. Rep.*, vol. 5, no. 1, pp. 1–8, 2015.
[10] G. Wang, D. L. Snyder, J. A. O'Sullivan, and M. W. Vannier, "Iterative deblurring for CT metal artifact reduction," *IEEE Trans. Med. Imag.*, vol. 15, no. 5, pp. 657–664, Oct. 1996.
[11] M. Beister, D. Kolditz, and W. A. Kalender, "Iterative reconstruction methods in X-ray cT," *Physica Medica*, vol. 28, no. 2, pp. 94–108, 2012.
[12] R. Gordon, R. Bender, and G. T. Herman, "Algebraic reconstruction techniques (ART) for three-dimensional electron microscopy and X-ray photography," *J. Theor. Biol.*, vol. 29, no. 3, pp. 471–481, 1970.
[13] H. Abeida, Q. Zhang, J. Li, and N. Merabtine, "Iterative sparse asymptotic minimum variance based approaches for array processing," *IEEE Trans. Signal Process.*, vol. 61, no. 4, pp. 933–944, Feb.15, 2013.
[14] J. A. Fessler, "Penalized weighted least-squares image reconstruction for positron emission tomography," *IEEE Trans. Med. Imag.*, vol. 13, no. 2, pp. 290–300, Jun. 1994.
[15] J. Adler and O. Öktem, "Learned primal-dual reconstruction," *IEEE Trans. Med. Imag.*, vol. 37, no. 6, pp. 1322–1332, Jun. 2018.
[16] H. Chen *et al.*, "LEARN: Learned experts' assessment-based reconstruction network for sparse-data cT," *IEEE Trans. Med. Imag.*, vol. 37, no. 6, pp. 1333–1347, Jun. 2018.
[17] T. Correia *et al.*, "Accelerated optical projection tomography applied to in vivo imaging of zebrafish," *PLoS One*, vol. 10, no. 8, 2015, Art. no. e0136213.
[18] H. M. Hudson and R. S. Larkin, "Ordered subsets of projection data," *IEEE Trans. Med. Imag.*, vol. 13, no. 4, pp. 601–609, Dec. 1994.
[19] C. Ghetti, O. Ortenzia, and G. Serreli, "CT iterative reconstruction in image space: A phantom study," *Phys. Medica*, vol. 28, no. 2, pp. 161–165, 2012.
[20] H. M. Hudson and R. S. Larkin, "Accelerated image reconstruction using ordered subsets of projection data," *IEEE Trans. Med. Imag.*, vol. 13, no. 4, pp. 601–609, Dec. 1994.
[21] L. A. Shepp and Y. Vardi, "Maximum likelihood reconstruction for emission tomography," *IEEE Trans. Med. Imag.*, vol. 1, no. 2, pp. 113–122, Oct. 1982.
[22] O. Ronneberger, O. P. Fischer, and T. Brox, "U-Net: Convolutional networks for biomedical image segmentation," in *Proc. Int. Conf. Medical Image Comput. Computer-Assisted Intervention*, Springer, Cham, 2015, pp. 234–241.
[23] Y. Guo, Z. Xiong, and F. J. Verbeek, "An efficient and robust hybrid method for segmentation of zebrafish objects from bright-field microscope images," *Mach. Vis. Appl.*, vol. 29, no. 8, pp. 1211–1225, 2018.
[24] E. W. Weisstein, "Sigmoid function," *MathWorld - A Wolfram Web Resour*, 2006.
[25] D. R. Cox, "The regression analysis of binary sequences," *J. R. Statist. Soc. Ser. B*, vol. 20, no. 2, pp. 215–232, 1958.
[26] D. P. Kingma and J. L. Ba, "Adam: A method for stochastic optimization," in *Proc. 3rd Int. Conf. Learn. Represent.*, San Diego, 2015.
[27] RStudio. "Keras," *Cheat Sheet*, 2017.
[28] D. Stalling, M. Westerhoff, and H. C. Hege, "Amira: A highly interactive system for visual data analysis," The visualization handbook, vol. 38, pp. 749–67, 2005.
[29] B. W. Matthews, "Comparison of the predicted and observed secondary structure of T4 phage lysozyme," *Biochimica et Biophysica Acta (BBA)-Protein Structure*, vol. 405, no. 2, pp. 442–451, 1975.
[30] K. Becker, N. Jährling, S. Saghafi, R. Weiler, and H. U. Dodt, "Chemical clearing and dehydration of GFP expressing mouse brains," *PLoS One*, vol. 7, no. 3, 2012, Art. no. e33916.
[31] H. Kolesová, M. Čapek, B. Radochová, J. Janáček, and D. Sedmera, "Comparison of different tissue clearing methods and 3D imaging techniques for visualization of GFP-expressing mouse embryos and embryonic hearts," *Histochem. Cell Biol.*, vol. 146, no. 2, pp. 141–152, 2016.
[32] X. Tang, G. E. M. Lamers, and F. J. Verbeek, "3D Image quality improvement for optical projection tomography via point spread function modelling," in *Proc. Imag. Appl. Opt. 2018 OSA Tech. Dig.; Opt. Soc. America*, 2018, Paper 3W5G.5.
[33] S. He *et al.*, "Synergy between loss of NF1 and overexpression of MYCN in neuroblastoma is mediated by the GAP-related domain," *Elife*, vol. 5, 2016, Art. no. e14713.
[34] V. Kantae *et al.*, "Pharmacokinetic modeling of paracetamol uptake and clearance in zebrafish larvae: Expanding the allometric scale in vertebrates with five orders of magnitude," *Zebrafish*, vol. 13, no. 6, pp. 504–510, 2016.
[35] R. C. van Wijk *et al.*, "Impact of post-hatching maturation on the pharmacokinetics of paracetamol in zebrafish larvae," *Sci. Rep.*, vol. 9, no. 1, pp. 1–9, 2019.
[36] R. C. Van Wijk, E. H. J. Krekels, V. Kantae, A. Ordas, and P. H. van der, Graaf, "Mechanistic and quantitative understanding of pharmacokinetics in zebrafish larvae through nanoscale blood sampling and metabolite modeling of paracetamol," *J. Pharmacol. Exp. Ther.*, vol. 372, no. 1, pp. 15–24, 2019.
[37] Council Directive 2010/63/EU. Council Directive 2010/63/EU protection animals used for Sci. purposes, 2010.

Xiaoqin Tang received the Ph.D. degree from the Bioimaging and Bioinformatics Group, Leiden Institute of Advanced Computer Science, Leiden University, Leiden, The Netherlands. She is currently a Postdoctoral Researcher with the same group at Leiden University. Her current research interest includes acquiring optimized 3-D reconstructed images from optical projection tomography and analyzing 3-D images to help identify and localize tumour, protein and/or gene in zebrafish.

Hermes A. J. Spaink received the M.Sc. degree in bioinformatics from Leiden University, Leiden, The Netherlands, in 2020 and the Ph.D. degree in neuroscience applying machine learning and AI. His research interest includes biological data analysis and machine learning, with a focus on genetics.

Rob C. van Wijk received the Ph.D. degree in systems pharmacology (systems biomedicine and pharmacology group) from Leiden University, Leiden, The Netherlands, in 2020. He is a Postdoctoral Researcher in pharmacometrics with the Department of Pharmaceutical Biosciences, Uppsala University, Sweden. His research interest includes translational pharmacology and predicting drug efficacy and safety from the preclinical to the clinical context, with a focus on integrating experimental and computational innovative methods.

Fons J. Verbeek received the Ph.D. degree in applied physics (pattern recognition group) from Delft University of Technology, Delft, The Netherlands, in 1995. He is currently a Full Professor in computational bioimaging with the Leiden Institute of Advanced Computer Science, Leiden University, The Netherlands. The zebrafish model system is used in a range of different application areas in his research. His research interest includes development of robust methods for large-scale image processing and analysis in the biosciences.